Acta Crystallographica Section B
Structural Science
ISSN 0108-7681

Systematic *ab initio* study of the compressibility of silicate garnets

V. Milman,[a]* E. V. Akhmatskaya,[b] R. H. Nobes,[b] B. Winkler,[c] C. J. Pickard[c] and J. A. White[a]

[a]Molecular Simulations Inc., The Quorum, Barnwell Road, Cambridge CB5 8RE, England, [b]Fujitsu European Centre for Information Technology, 2 Longwalk Road, Stockley Park, Uxbridge UB11 1AB, England, and [c]Institut für Geowissenschaften, Mineralogie/Kristallographie, Olshausenstrasse 40, D 24098 Kiel, Germany

Correspondence e-mail: vmilman@msi-eu.com

Received 18 August 2000
Accepted 21 November 2000

The structural properties of the silicate garnets andradite, $Ca_3Fe_2Si_3O_{12}$, uvarovite, $Ca_3Cr_2Si_3O_{12}$, knorringite, $Mg_3Cr_2Si_3O_{12}$, goldmanite, $Ca_3V_2Si_3O_{12}$, blythite, $Mn_3^{2+}Mn_2^{3+}Si_3O_{12}$, skiagite, $Fe_3^{2+}Fe_2^{3+}Si_3O_{12}$, calderite, $Mn_3^{2+}Fe_2^{3+}Si_3O_{12}$, and khoharite, $Mg_3Fe_2^{3+}Si_3O_{12}$, have been investigated with a quantum-mechanical model as a function of applied pressure. The study has been performed with the density functional theory code CASTEP, which uses pseudopotentials and a plane-wave basis set. All structural parameters have been optimized. The calculated static geometries (cell parameters, internal coordinates of atoms and bond lengths), bulk moduli and their pressure derivatives are in good agreement with the experimental data available. Predictions are made for those cases where no experimental data have been reported. The data clearly indicate that the elastic properties of all silicate garnets are dominated by the compressibility of the dodecahedral site. The compression mechanism is found to be based on a bending of the angle between the centers of the SiO_4 tetrahedra and the adjacent octahedra, as in the aluminosilicate garnets. An analysis of the relationship between ionic radii of the cations and the compressibility of silicate garnets is presented.

1. Introduction

The crystal chemistry of garnets, and especially silicate garnets, has long attracted the attention of mineralogists and crystallographers (Geller, 1967; Novak & Gibbs, 1971). Most garnets crystallize in the body-centered cubic space group $Ia\bar{3}d$ and the present study is restricted to such structures. There are $Z = 8$ formula units $X_3Y_2Si_3O_{12}$ per unit cell of a silicate garnet, *i.e.* there are 160 atoms per conventional unit cell. The structure can be described as consisting of chains in which corner-sharing SiO_4 tetrahedra and YO_6 octahedra alternate (Fig. 1). Each tetrahedron shares its corners with four different YO_6 octahedra, while each octahedron is corner-linked to six different tetrahedra. A third type of coordination polyhedron is the triangular dodecahedron occupied by the X cations. The Si atoms and the cations Y = Al, Fe, Mn, Cr, V and X = Ca, Mg, Fe, Mn are located on Wyckoff positions 24(d), 16(a) and 24(c), respectively. These correspond to positions with fractional coordinates Si = (3/8, 0, $\frac{1}{4}$), Y = (0, 0, 0) and X = (0, $\frac{1}{4}$, 1/8). The oxygen occupies Wyckoff position 96(h) with coordinates (x, y, z) so that the end-member garnet structure is fully described by the three fractional coordinates of an O atom and the cell parameter.

The large family of silicate garnets offers the possibility to study systematically physical properties of isotypic compounds as a function of cation species incorporated into dodecahedral

© 2001 International Union of Crystallography
Printed in Great Britain – all rights reserved

and octahedral sites. However, systematic experimental studies of the properties of garnets as a function of their composition are difficult since natural samples are invariably solid solutions, and hence values for the physical properties of end-members have to be obtained by extrapolation. Synthetic samples are often not readily available, as many garnets can be synthesized only at high temperatures and pressures. Fermor (1938) made an early attempt to predict the existence of a number of garnets beyond those encountered in nature. Gentile & Roy (1960) presented probably the first large-scale attempt to synthesize a number of garnets that cannot be found naturally. These authors succeeded in producing a number of new compounds, including a silicate garnet $Cd_3Al_2Si_3O_{12}$. The synthesis of new chromium-containing garnets $Mn_3Cr_2Si_3O_{12}$ and $Fe_3Cr_2Si_3O_{12}$ was described by Fursenko (1980). The same author (Fursenko, 1983) produced a number of Mn-containing garnets $Mn_3M_2Si_3O_{12}$ (M = V, Mn, Ga). Two isostructural synthetic polymorphs of $Co_3Al_2Si_3O_{12}$ garnet have been reported (Ohashi *et al.*, 1981; Ohashi *et al.*, 1995), where the authors suggest that the spin state of the Co ions differs between the two polymorphs. Nishizawa *et al.* (1977) synthesized and studied the properties of Fe-containing garnets $M_3Fe_2Si_3O_{12}$ (M = Mn, Cd, Ca). While the list of such studies can be expanded, their contribution to a deeper understanding of the structure–property relations in garnets is limited, especially as mostly only cell parameters are reported.

An alternative way of studying various garnets is by using atomistic modeling, the so-called 'computational crystallography' approach (Winkler, 1999). It has been shown that a quantum-mechanical treatment based on density functional theory provides an accurate description of the structure and properties of complex inorganic solids (Winkler, 1999; Akhmatskaya *et al.*, 1999; Milman *et al.*, 2000). In the present study, we adopted this theoretical approach to study the dependence of the structure and properties of silicate garnets on the nature of X and Y cations.

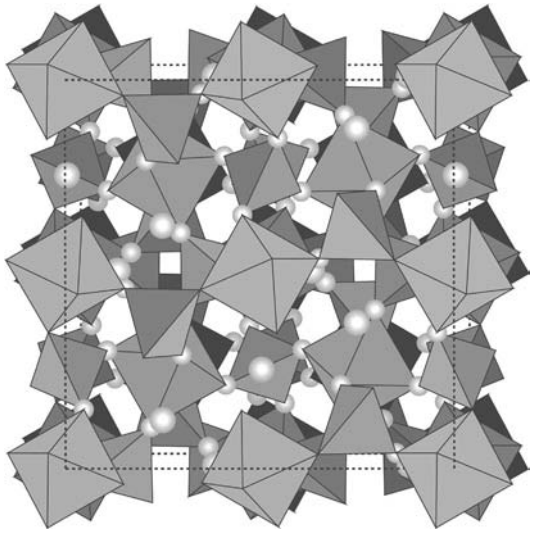

Figure 1
A representation of the garnet structure. Si ions occupy tetrahedra and trivalent cations occupy octahedra. Small spheres correspond to oxygen ions; larger spheres represent cations that occupy triangular dodecahedra.

The paper deals with the ground-state structure and the structure under pressure of a number of end-member garnets, namely andradite, $Ca_3Fe_2Si_3O_{12}$, uvarovite, $Ca_3Cr_2Si_3O_{12}$, knorringite, $Mg_3Cr_2Si_3O_{12}$, goldmanite, $Ca_3V_2Si_3O_{12}$, blythite, $Mn_3^{2+}Mn_2^{3+}Si_3O_{12}$, skiagite, $Fe_3^{2+}Fe_2^{3+}Si_3O_{12}$, calderite, $Mn_3^{2+}Fe_2^{3+}Si_3O_{12}$, and khoharite, $Mg_3Fe_2^{3+}Si_3O_{12}$. These results complement a previous theoretical study of the aluminosilicate garnets pyrope, $Mg_3Al_2Si_3O_{12}$, grossular, $Ca_3Al_2Si_3O_{12}$, almandine, $Fe_3Al_2Si_3O_{12}$, and spessartine, $Mn_3Al_2Si_3O_{12}$ (Akhmatskaya *et al.*, 1999). We paid particular attention to pressure-induced structural changes since these depend on the relative strengths of the interatomic interactions. High-pressure studies are especially well suited to study the effect of cation substitution, as even at moderate pressures differences in the pressure-induced structural changes between isotypic compounds are much larger than temperature-induced ones. Hence, differences in structure–property relationships between isotypic structures are enhanced at high pressures with respect to the corresponding differences at ambient pressure.

2. Computational details

The quantum-mechanical calculations performed here are based on density functional theory, DFT (Hohenberg & Kohn, 1964; Kohn & Sham, 1965). Exchange–correlation effects were taken into account using the spin-polarized form of the generalized gradient approximation, GGA (Perdew & Wang, 1992), as implemented by White & Bird (1994). The total energy code *CASTEP* (Molecular Simulations Inc., 1998; Milman *et al.*, 2000) was used, which utilizes pseudopotentials to describe electron–ion interactions and represents electronic wavefunctions using a plane-wave basis set (Payne *et al.*, 1992). An energy cutoff of 380 eV and a single Γ point sampling of the Brillouin zone were found to produce converged results for all structural parameters. We used ultrasoft pseudopotentials (Vanderbilt, 1990) which require significantly less computational resources than norm-conserving potentials (Lin *et al.*, 1993).

It has been shown that an accurate description of the interaction between core and valence electrons is needed in spin-density calculations (Louie *et al.*, 1982), especially when transition-metal ions are involved. It appears that the best way to satisfy this condition for Cr and V is to treat 3*s* and 3*p* electrons as valence electrons when constructing pseudopotentials. This treatment is not necessary for the heavier elements Fe and Mn. These pseudopotentials are sufficiently accurate when 3*s* and 3*p* electrons are treated as part of the core, and the overlap of core and valence charge densities is accounted for by introducing non-linear core correction terms (Louie *et al.*, 1982). The transferability and accuracy of all of the above pseudopotentials was illustrated by Milman *et al.* (2000).

A primitive cell comprising 80 atoms is used in the calculations reported here. This speeds up the calculations

Table 1
Structure of andradite at ambient pressure: cell parameter, fractional coordinates of the O atom, and bond lengths.

	Theory	Experiment[(a)]	Experiment[(b)]	Experiment[(c)]	Experiment[(d)]	Experiment[(e)]
a (Å)	12.058	12.051 (1)	12.045 (1)	12.058 (1)	12.0643 (3)	12.061 (1)
O_x	0.0403	0.03914 (6)	0.0395 (2)	0.03986 (15)	0.03932 (2)	0.0383 (4)
O_y	0.0467	0.04895 (6)	0.0488 (1)	0.04885 (13)	0.04863 (4)	0.0472 (4)
O_z	0.6561	0.65534 (6)	0.6556 (1)	0.65555 (15)	0.65537 (4)	0.6535 (4)
Fe—O (Å)	2.024	2.0186 (7)	2.016 (2)	2.024 (2)	2.021 (1)	1.991 (1)
Si—O (Å)	1.626	1.6492 (7)	1.643 (2)	1.643 (2)	1.648 (1)	1.665 (1)
Ca—O(1) (Å)	2.360	2.3584 (7)	2.358 (2)	2.366 (2)	2.362 (1)	2.358 (1)
Ca—O(2) (Å)	2.527	2.4953 (7)	2.494 (2)	2.500 (2)	2.502 (1)	2.513 (1)

(*a*) Ambruster & Geiger (1993), 100 K; (*b*) Hazen & Finger (1989); (*c*) Novak & Gibbs (1971); (*d*) Pilati *et al.* (1996); (*e*) Quareni & de Pieri (1966).

considerably compared with the calculations for the conventional cell with 160 atoms, since the scaling of the pseudopotential plane-wave method with the number of atoms, N, is between N^2 and N^3 (Payne *et al.*, 1992). Geometry optimizations at zero pressure were performed with the variable lattice parameter and full relaxation of the internal coordinates. Calculations were considered to be converged when the maximum force on an atom was below 0.01 eV Å^{-1}.

There are two ways of applying quantum-mechanical models to high-pressure studies. The most obvious technique is to calculate the equation-of-state by following the same methodology as in the actual experiment. One would apply an external hydrostatic pressure to the system, optimize cell parameters and internal degrees of freedom and thus obtain a single P–V point for the theoretical equation-of-state. A full equation-of-state could be constructed by repeating this process at a number of fixed pressure values. There exists an alternative protocol which is applicable for crystals with cubic symmetry. It is possible in this case to fix volume rather than pressure, *i.e.* to perform minimization of internal coordinates for a set of fixed cell constants, and to calculate the pressure for each minimized structure. The latter approach, which we used in the present work, is faster since it avoids the cell optimization step. The resultant P–V data sets were fitted with a third-order Birch–Murnaghan equation-of-state (Birch, 1978) to obtain the bulk moduli, B, and their pressure derivatives, B'. All calculations were performed on a Fujitsu VX vector processor.

3. Garnet properties: ground state and compressibility

3.1. Andradite

Calculated structural parameters for andradite ($Ca_3Fe_2Si_3O_{12}$) at ambient pressure are presented in Table 1. The computed unit-cell parameter of 12.058 Å agrees to within 0.1% with the result of an accurate low-temperature single-crystal X-ray study carried out on synthetic andradite (Armbruster & Geiger, 1993). A value of 12.068 (2) Å has been reported for synthetic andradite from a powder diffraction study (Wang *et al.*, 1999) and further experimental data are listed in Table 1 for comparison. Recent experiments on single crystals of natural garnets with 91.5% (Conrad *et al.*, 1999) and 94% (Kingma & Downs, 1989) andradite content gave a slightly smaller unit-cell parameter of 12.048 (1) Å.

Our calculations were carried out for the high-spin state of the Fe ions and within the gradient-corrected version of the spin-density functional we obtained a ferromagnetic ground state for andradite. We have not attempted to decrease the symmetry of the system and search for an antiferromagnetic solution. It has been shown experimentally that andradite orders antiferromagnetically at 11.5 (1) K (Murad, 1984). The very low value of the Néel temperature suggests that magnetic effects should not have an important effect on the structural properties of andradite.

The calculated equation-of-state up to 100 GPa is compared with the experimental data in Fig. 2. A high-pressure single-crystal study of andradite (Hazen & Finger, 1989) presents a rare source of experimental information on the compression mechanism of the garnet structure. One should bear in mind, however, that the highest-pressure results from that study are likely to have been collected under nonhydrostatic conditions. It has been shown recently (Sinogeikin & Bass, 1999) that even slight deviations from hydrostatic conditions can lead to an error of approximately 2% in the estimated bulk modulus of a mineral. We obtained B = 147.1 (4) GPa and B' = 4.41 (2) from the calculated equation-of-state shown in Fig. 2. Hazen & Finger (1989) derived B = 159 (2) GPa from the second-order Birch–Murnaghan equation-of-state (assuming a fixed value of B' = 4). Bass (1986) measured single-crystal elastic prop-

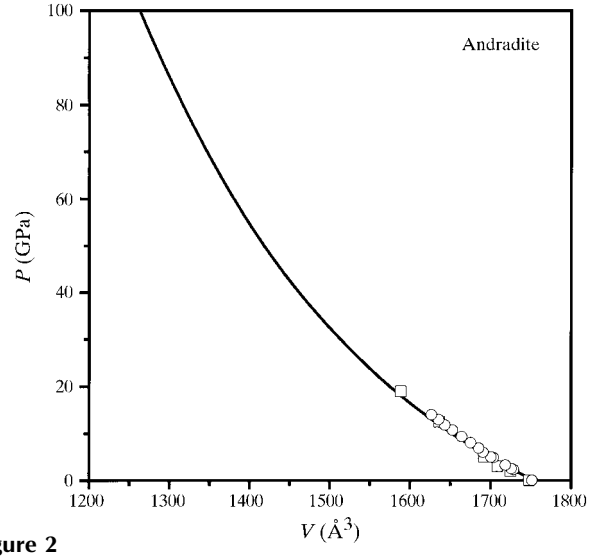

Figure 2
Equation-of-state for andradite; symbols refer to experiment (squares: Hazen & Finger, 1989; circles: Zhang *et al.*, 1999) and the solid line to the present calculation.

erties of a similar natural garnet containing 96% andradite and obtained B = 158 (2) GPa from Brillouin spectroscopy results. A recent high-pressure Brillouin scattering study of a natural garnet containing 91.5% andradite (Conrad *et al.*, 1999) gave B = 159.38 GPa and B' = 5.85. It is difficult to quantify how much of the discrepancy between the theoretical and experimental values for the bulk modulus is due to the deviation from end-member stoichiometry in the samples used in the experiments. Babuska *et al.* (1978) and Leitner *et al.* (1980) have extrapolated a value of B = 140 GPa for pure andradite using experimental data for garnet solid solutions. However, a 10% disagreement is usually judged as acceptable in DFT calculations.

The low accuracy of the experimentally determined bond lengths in andradite under pressure can be inferred from Fig. 3. There are altogether five experimental points at nonzero pressures. Hazen & Finger (1989) have described the point at 2 GPa as unreliable and indeed it does not follow a generally smooth pressure dependence of the Ca—O and Fe—O bond lengths. The points at 12.5 and 19 GPa correspond to non-hydrostatic conditions where significant distortions from cubic symmetry were observed (Hazen & Finger, 1989). The remaining experimental data do not provide sufficient information to study the compression mechanism.

Here, and for the garnets discussed below, we predict the compression behavior over a range of 100 GPa. It has been shown that the compression mechanism of aluminosilicate garnets is determined to a large extent by the change in the Si—O—Al angle (Akhmatskaya *et al.*, 1999). This is best illustrated by the linear correlation between the normalized polyhedral distortion indices (Baur, 1974; Renner & Lehmann, 1986) and the relative change of the Si—O—Y angle in the garnet structure. We have found that such correlation in andradite (Fig. 4) is qualitatively similar to the results for spessartine (Akhmatskaya *et al.*, 1999). The pressure dependence of calculated and measured (Hazen & Finger, 1989) polyhedral distortion indices in andradite is shown in Fig. 5. All polyhedra in andradite become more regular on compression up to 30 GPa. Further compression changes the sense of the distortion of the FeO_6 octahedra, which become irregular again. The experimental data on polyhedral distortions exhibit significant scatter, but there is nevertheless good agreement between the calculated results and those derived from the refined structures given by Hazen & Finger (1989). These data further confirm that the structure refinement at the highest pressure of 19 GPa achieved by Hazen & Finger (1989) is unreliable.

Table 2
Structure of uvarovite at ambient pressure: cell parameters, fractional coordinates of the O atom and bond lengths.

	Theory	Experiment[(a)]	Experiment [(b)]
a (Å)	12.021	12.0205 (5)	11.988 (1)
O_x	0.0403	0.0396 (5)	0.03991 (16)
O_y	0.0460	0.0472 (5)	0.04737 (15)
O_z	0.6554	0.6559 (4)	0.65354 (17)
Cr—O (Å)	2.008	2.015 (5)	1.985 (2)
Si—O (Å)	1.623	1.630 (6)	1.643 (2)
Ca—O(1) (Å)	2.355	2.349 (6)	2.360 (2)
Ca—O(2) (Å)	2.526	2.511 (6)	2.499 (2)

(*a*) Carda *et al.* (1994); (*b*) Novak & Gibbs (1971), natural garnet containing 87% uvarovite.

3.2. Uvarovite

Calculated structural parameters for uvarovite ($Ca_3Cr_2Si_3O_{12}$) are compared with experimental results in Table 2. Carda *et al.* (1994) refined the structure of a family of synthetic uvarovite–grossular solid solutions, including pure end-members. Our data for the unit-cell parameters, internal

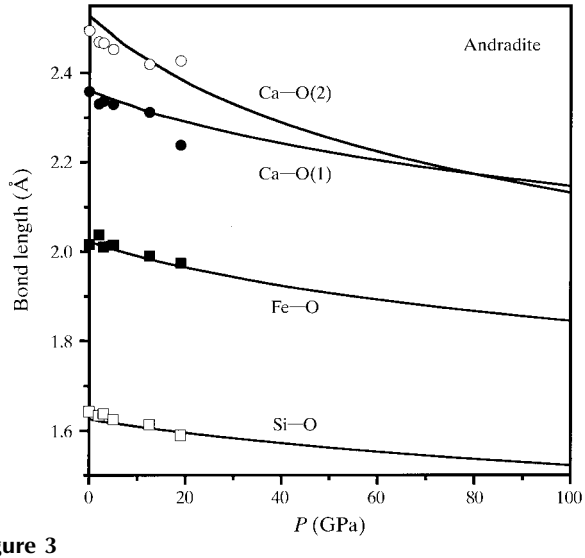

Figure 3
Calculated pressure dependence of bond lengths in andradite; symbols refer to experiment (Hazen & Finger, 1989) and solid lines to the present calculation.

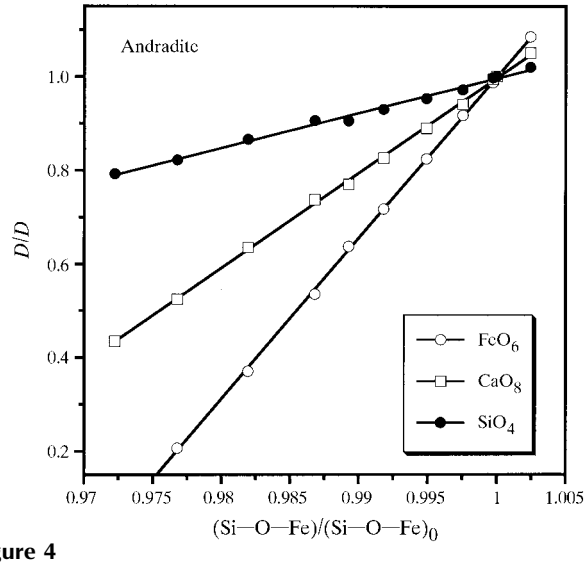

Figure 4
Dependence of the normalized polyhedral distortion parameters in andradite on the relative change of the Si—O—Fe angle. Bond length distortion was used for CaO_8, edge-length distortion for FeO_6 and angular distortion for SiO_4. Symbols refer to the calculated values and lines to a linear fit.

coordinates and bond lengths are in excellent agreement with their experimental findings for pure uvarovite, see Table 2. The cell parameter of uvarovite of 12.02 Å as derived from both experiment and theory is consistent with a structural analysis of garnets based on ionic radii. This value is roughly 0.03 Å smaller than the cell parameter of andradite, see Table 1, which is the difference between the ionic radii of trivalent Fe and Cr ions (Shannon, 1976). Note that, as in the case of andradite, the calculations were performed for the high-spin state of the transition-metal ion, and the gradient-corrected spin-density approximation resulted in the ferromagnetic ground state.

The calculated equation-of-state up to 100 GPa is shown in Fig. 6 in comparison to experimental data determined by powder X-ray diffraction in a diamond anvil cell (Leger *et al.*, 1990). The experimental results shown in Fig. 6 can be divided into two pressure regions. The high-pressure data were obtained in a solidified pressure-transmitting medium, which caused significant nonhydrostatic effects and resulted in large data scatter for $P > 10$ GPa. The low-pressure data are more consistent and agree very well with the calculated equation-of-state. Leger *et al.* (1990) considered their data not to be reliable enough to fit a third-order Birch–Murnaghan equation-of-state and to determine both the bulk modulus and its pressure derivative. Instead, they have chosen to fix the bulk modulus value to 162 (2) GPa, as measured by Brillouin spectroscopy on a small synthetic crystal (Bass, 1986). The subsequent fitting of the experimental data with the fixed value of B produced $B' = 4.7$ (7). The theoretical results are $B = 143$ (1) GPa and $B' = 4.73$ (18), *i.e.* the computed bulk modulus is almost 20 GPa smaller than the experimentally determined value. This is a very unusual result since for all other garnets examined here and in the earlier paper (Akhmatskaya *et al.*, 1999), the discrepancy between experimental and theoretical bulk modulus did not exceed 10–11 GPa. The Brillouin spectroscopy study (Bass, 1986) is the only experimental work that reports the bulk modulus for uvarovite. Earlier estimates based on the data for solid-solution series predicted B to be in the range 134–168 GPa (Leitner *et al.*, 1980). We re-examined the static compression data by Leger *et al.* (1990) and fitted their low-pressure subset of data using a third-order Birch–Murnaghan equation-of-state with B' fixed to 4.7. The chosen value for B' is consistent with both the theoretical prediction and the analysis of the complete experimental data set (Leger *et al.*, 1990). This fit gave $B = 144$ (8) GPa, in good agreement with the calculated bulk modulus. It therefore appears that further measurements are desirable to determine accurately the bulk modulus and its pressure derivative for uvarovite.

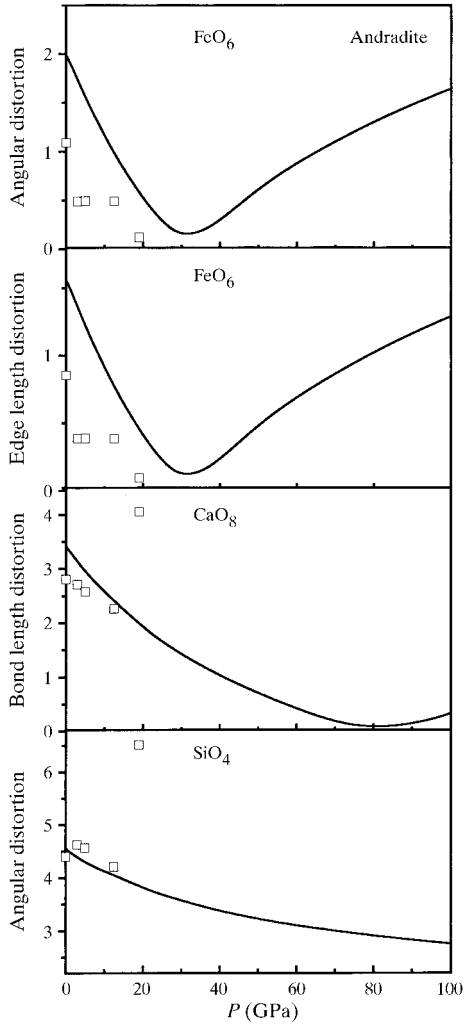

Figure 5
Pressure dependence of polyhedral distortions in andradite; squares refer to experiment (Hazen & Finger, 1989) and solid lines to the present calculation.

3.3. Goldmanite

Goldmanite ($Ca_3V_2Si_3O_{12}$), the vanadium analogue of grossular and andradite, occurs rarely in nature. Goldmanite–grossular solid solutions with a content of goldmanite as high as 68% have been found within metamorphosized calcareous metapelites (Benkerrou & Fonteilles, 1989). The cell para-

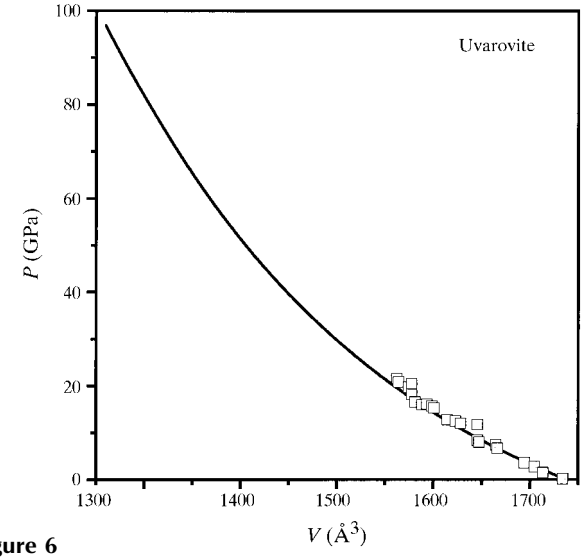

Figure 6
Equation-of-state for uvarovite; squares refer to experiment (Leger *et al.*, 1990) and the solid line to the present calculation.

Table 3
Structure of goldmanite at ambient pressure: cell parameters, fractional coordinates of the O atom and bond lengths.

Calculated column is based on the equations from Novak & Gibbs (1971) with ionic radii 1.12 Å for Ca and 0.64 Å for V (Shannon, 1976).

	Theory	Experiment[(a)]	Calculated
a (Å)	12.080	12.011 (1)	12.05
O_x	0.0409	0.03850 (20)	0.0395
O_y	0.0464	0.04742 (20)	0.0484
O_z	0.6561	0.65387 (18)	0.6548
V—O (Å)	2.028	1.988 (2)	2.012
Si—O (Å)	1.623	1.655 (2)	1.649
Ca—O(1) (Å)	2.370	2.348 (3)	2.363
Ca—O(2) (Å)	2.534	2.501 (2)	2.501

(*a*) Novak & Gibbs (1971), natural garnet, goldmanite content 60%.

meter of the solid solution with 54% goldmanite content was reported as 11.971 (2) Å and these authors provided no further structural data. Hallsworth *et al.* (1992) found goldmanite as a detrital grain in sandstone of Palaeocene age. The grain contained 96.3% of the goldmanite end-member and is the purest natural goldmanite analyzed to date. The cell parameter was determined as 12.06 Å. Very recently, goldmanite was found in the carbonaceous black slates in the Ogcheon belt in Korea (Jeong & Kim, 1999), with a content of goldmanite as high as 91%. The cell parameter of 12.04 Å that was reported for this sample is consistent with the variation of the cell dimensions in the grossular–goldmanite solid–solution series. Synthetic goldmanite has been obtained by Mill' (1964), Strens (1965) and Geller (1967), who reported lattice parameters of 12.09, 12.070 (5) and 12.068 Å, respectively.

The only known attempt at refining the atomic structure of goldmanite was made on a sample containing only 60% of this component (Novak & Gibbs, 1971). In addition to the quantum-mechanical modeling, we have therefore calculated the structural parameters of pure goldmanite based on the empirical correlations between the structure and ionic radii of cations as derived by Novak & Gibbs (1971). As can be seen from the results in Table 3, the cell parameter calculated from first principles, 12.080 Å, and the empirically predicted value of 12.05 Å are both close to the experimental value.

The bulk modulus of goldmanite and its pressure derivative were calculated as 139.4 (9) GPa and 4.69 (7), respectively. The pressure dependence of the bond lengths is presented in Fig. 7. The two symmetrically inequivalent Ca—O bonds become metrically equal at approximately 70 GPa.

The general pattern of structural changes in goldmanite under compression is very similar to that for andradite and uvarovite. The compressibilities of the Ca—O and Si—O bond lengths in these garnets are practically identical (see Fig. 7). In addition, the pressure dependence of polyhedral distortions is very similar in goldmanite, andradite and uvarovite, as illustrated by Fig. 8. All polyhedra in goldmanite become more regular on compression up to 40 GPa. The VO_6 octahedra change the sense of distortion at higher pressures and become more irregular upon further compression. The linear correlation between the normalized distortion indices and the change of the Si—O—Y angle in goldmanite is similar to the results

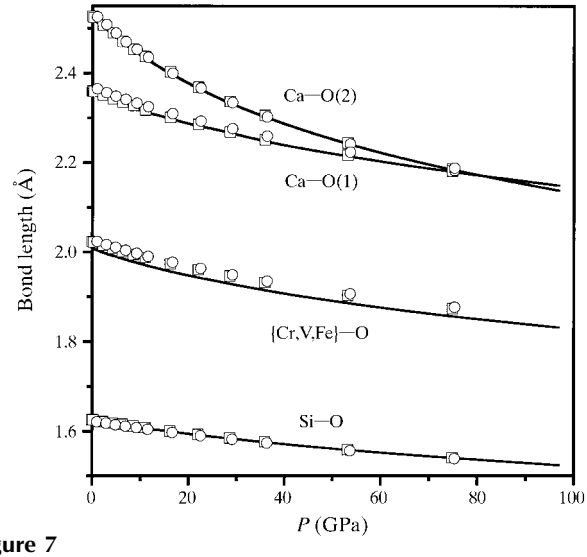

Figure 7
Calculated pressure dependence of bond lengths in uvarovite (solid lines), andradite (squares) and goldmanite (circles).

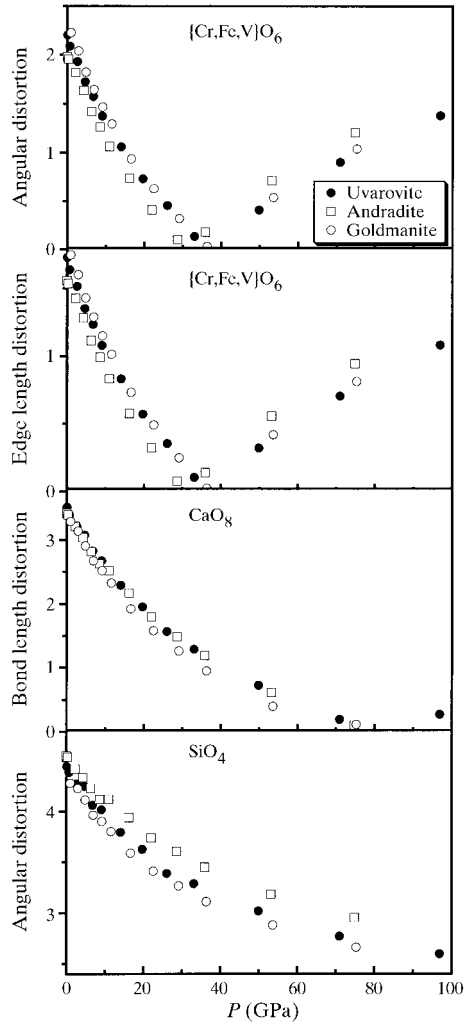

Figure 8
Pressure dependence of bond lengths in uvarovite (solid circles), andradite (squares) and goldmanite (open circles).

Table 4
Structure of knorringite at ambient pressure: cell parameters, fractional coordinates of the O atom and bond lengths.

	Theory	Experiment[(a)]	Calculated[(b)]
a (Å)	11.646	11.526 (1)	11.64
O_x	0.0353	0.03346 (9)	0.0343
O_y	0.0521	0.0507 (1)	0.0528
O_z	0.6575	0.65336 (9)	0.6560
Cr—O (Å)	1.976	1.905 (1)	1.96
Si—O (Å)	1.618	1.639 (1)	1.64
Mg—O(1) (Å)	2.239	2.216 (1)	2.24
Mg—O(2) (Å)	2.372	2.353 (1)	2.36

(*a*) Novak & Gibbs (1971), natural garnet, knorringite content 28.5%; (*b*) Novak & Gibbs (1971), prediction based on the empirical formula.

for uvarovite, andradite (Fig. 4) and spessartine (Akhmatskaya *et al.*, 1999). It appears that Fe, Cr and V divalent cations play an almost identical role in the garnet structure, which is consistent with the fact that their ionic radii are very close.

3.4. Knorringite

Knorringite garnet, $Mg_3Cr_2Si_3O_{12}$, can account for up to 50% of garnet inclusions in natural diamonds (Irifune *et al.*, 1982). This garnet is expected to be an important component in deeper parts of the upper mantle. Knorringite is unstable on heating at ambient pressure, which explains experimental difficulties encountered during the synthesis of the pure end-member. Ringwood (1977) and Irifune *et al.* (1982) reported the lattice parameter of synthetic knorringite as 11.600 (1) and 11.596 (1) Å, respectively. The calculated lattice parameter, 11.646 Å, is larger by 0.4%. Novak & Gibbs (1971) predicted a lattice parameter of 11.64 Å for pure knorringite, see Table 4, which is again in good agreement with both experiment and the quantum-mechanical calculation.

The bulk modulus of knorringite is found to be 153.4 (9) GPa, with $B' = 4.34$ (8). The pressure dependence of the bond lengths is illustrated in Fig. 9. The two Mg—O bond lengths become equal at a relatively low pressure of 50 GPa compared with 70–75 GPa in goldmanite, andradite and uvarovite (Fig. 7), 75 GPa in almandine, 100 GPa in pyrope, 105 GPa in spessartine and 135 GPa in grossular (Akhmatskaya *et al.*, 1999).

The pressure dependence of the polyhedral distortion indices is presented in Fig. 10 in comparison with khoharite data and with earlier results for pyrope (Akhmatskaya *et al.*, 1999).

3.5. Khoharite

The first description of khoharite, $Mg_3Fe_2^{3+}[SiO_4]_3$, as a member of the garnet family apparently belongs to Fermor (1938). He based his analysis on the data obtained from the Khohar meteorite and on the previously published analysis of a red garnet from the Jagersfontein diamond mine in South Africa. Coes (1955) later reported the successful high-pressure synthesis of khoharite as well as of knorringite and calderite.

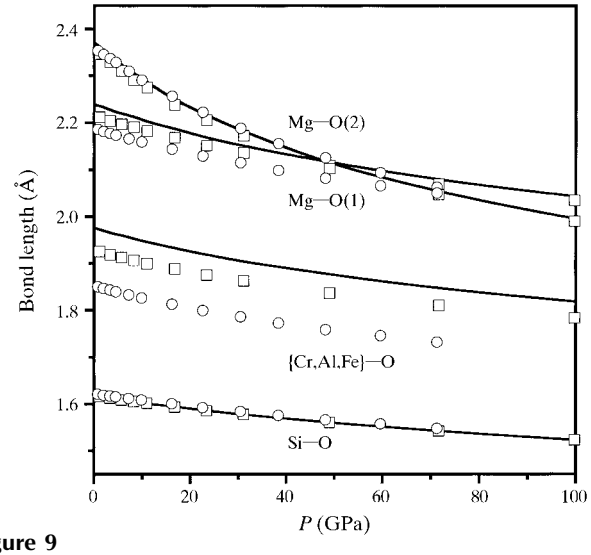

Figure 9
Calculated pressure dependence of bond lengths in knorringite (solid lines), khoharite (squares) and pyrope (circles, from Akhmatskaya *et al.*, 1999).

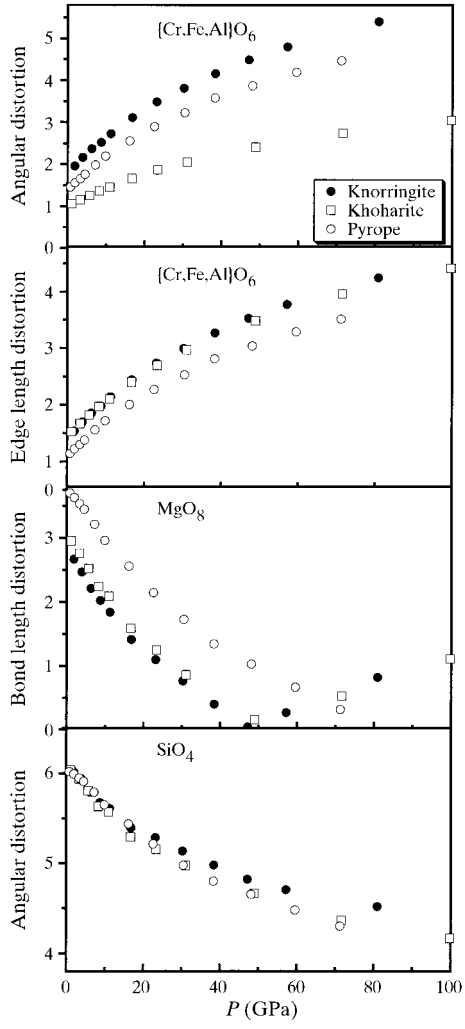

Figure 10
Pressure dependence of polyhedral distortions in knorringite (solid circles), khoharite (squares) and pyrope (open circles, from Akhmatskaya *et al.*, 1999).

Table 5
Structure of khoharite at ambient pressure: cell parameters, fractional coordinates of the O atom and bond lengths.

	Theory	Calculated[(a)]
a (Å)	11.525	11.69
O_x	0.0345	0.0347
O_y	0.0509	0.0539
O_z	0.6555	0.6570
Fe^{3+}—O (Å)	1.927	1.98
Si—O (Å)	1.618	1.64
Mg—O(1) (Å)	2.215	2.25
Mg—O(2) (Å)	2.354	2.36

(*a*) Novak & Gibbs (1971), empirical extrapolation.

Table 6
Structure of blythite at ambient pressure: cell parameters, fractional coordinates of the O atom and bond lengths.

	Theory	Experiment[(a)]
a (Å)	11.897	11.788 (2)
O_x	0.0378	0.0363 (3)
O_y	0.0526	0.0526 (3)
O_z	0.6594	0.6570 (3)
Mn^{3+}—O (Å)	2.047	1.998 (3)
Si—O (Å)	1.622	1.636 (3)
Mn^{2+}—O(1) (Å)	2.304	2.280 (4)
Mn^{2+}—O(2) (Å)	2.423	2.396 (3)

(*a*) Arlt *et al.* (1998), 100 K.

Unfortunately, neither of these authors provided any structural information on khoharite. Novak & Gibbs (1971) have predicted the structure of khoharite and we are not aware of any other detailed study of this garnet. The ground-state properties of khoharite as calculated here are: a = 11.525 Å, B = 162.9 (9) GPa, B' = 4.43 (3). Details of the predicted structure are given in Table 5 in comparison with the empirical results of Novak & Gibbs (1971). Khoharite is the only garnet out of all those investigated here and in the related study (Akhmatskaya *et al.*, 1999) where DFT–GGA predicts a noticeably lower lattice constant than that given by Novak & Gibbs (1971). Polyhedral distortions for khoharite are compared with the results for knorringite and pyrope in Fig. 10. The qualitative description is the same in these three garnets: YO_6 octahedra become more distorted on compression, starting from ambient pressure, while tetrahedra and dodecahedra become more regular.

3.6. Blythite

The garnet end-member blythite with composition $Mn_3^{2+}Mn_2^{3+}[SiO_4]_3$ is of interest as it is one of the few mixed-valence garnets and it was thought that Jahn–Teller distortions may lead to a cubic to tetragonal phase transition, similar to the transition observed in $Ca_3Mn_2^{3+}[GeO_4]_3$. Experimental results clearly indicate, however, that $Mn^{3+}$and Fe^{3+} ions do not cause a lowering of the space-group symmetry due to ordered static Jahn–Teller distortions of the octahedron in the silicate garnets (Arni *et al.*, 1985). Arlt *et al.* (1998) concluded that unusually large anisotropic displacement parameters of the O atoms were indicative of dynamically or statically disordered Jahn–Teller distortions.

The model used in the present study cannot be adapted to study disordered structures without requiring prohibitively large amounts of computing time. However, a comparison of the theoretical values with those measured by Arlt *et al.* (1998), who presented the first accurate structure determination of synthetic blythite crystals including low-temperature and high-pressure measurements, shows that the agreement is within the usual accuracy of the approach used here. The computed cell parameter, 11.897 Å, is overestimated by 0.9% compared with the low-temperature value of 11.788 (2) Å reported by Arlt *et al.* (1998), see Table 6. The overestimation of the theoretical value might be partially due to the fact that experiments refer to the paramagnetic phase. It seems that the proposed dynamic or static disordered Jahn–Teller distortions do not cause a significant change of the lattice parameters. This is confirmed by an estimate of the lattice parameter based on the empirical formulae of Novak & Gibbs (1971) with the effective ionic radii from Shannon (1976), which gives 11.80 Å in slightly better agreement with the experimental value than the result obtained from the quantum-mechanical calculation.

The calculated bulk modulus, 150 (1) GPa, is in good agreement with the experimental result, 151.6 (8) GPa. The discrepancy between the calculated pressure derivative, B' = 4.76 (8), and the experimental value, 6.38, is however, larger than is usually the case. Generally, B' for silicate garnets is close to 4–4.5 and the comparisons in Table 7 indicate that significant deviations from this value are usually only encountered in older data, where results were derived from energy-dispersive measurements or where non-gasketed samples had been used or other experimental problems occurred. Although there is only one experimental datum available and hence the possibility of a systematic error cannot be completely excluded, we think that the high experimental value for B' may be attributed to the presence of the dynamically or statically disordered Jahn–Teller distorted dodecahedra. The disorder of the oxygen and the Mn^{3+} ions around their equilibrium sites in the ambient pressure structure would then be responsible for the comparatively large change of B as a function of pressure. Hence, the static quantum-mechanical model, where each atom occupies its equilibrium site and thermal motion is neglected, cannot be expected to reproduce this behavior.

3.7. Skiagite

Skiagite, $Fe_3^{2+}Fe_2^{3+}[SiO_4]_3$, represents another mixed-valence garnet end-member. As it has not yet been observed as a dominant component in a solid solution, all reported structural studies of skiagite have been carried out on synthetic samples that are produced by high-temperature/high-pressure synthesis. The first report of the synthesis of skiagite (Karpinskaya *et al.*, 1982) gave the cell parameter as 11.71 (5) Å and the authors found skiagite to form in the pressure range between 9 and 12 GPa. This cell parameter agrees well with the value of 11.72 Å predicted by Novak &

Table 7
Equilibrium cell volume, bulk modulus and its pressure derivative, bulk moduli for the individual polyhedra, and the relative volume of polyhedra in the cell.

Garnet $X_3Y_2Si_3O_{12}$	X	Y	V_0 (Å^3)	B (GPa)	B'	B_{SiO_4} (GPa)	V_{SiO_4} (%)	B_{YO_6} (GPa)	V_{YO_6} (%)	B_{XO_8} (GPa)	V_{XO_8} (%)
Pyrope[a]	Mg	Al	1479.6	170	4.3	391	2.32	204	9.2	127	33.0
exp.				173[b]	3.22[b]			275[c]			
				171[d]	4.4[d]	580[d]		211[d]		107[d]	
				171[e]	1.8[e]	300[f]		220[f]		130[f]	
				171[g]	5.3[g]						
				171[h]	4.4[h]						
Almandine[a]	Fe	Al	1524.6	177	4.2	434	2.27	213	9.0	121	33.9
exp.				175[e]	1.5[e]			123[i]			
				185[h]	4.2[h]						
				178[j]							
Spessartine[a]	Mn	Al	1567.3	183	3.9	327	2.24	182	8.9	141	34.5
exp.				179[k]							
				189[h]	4.2[h]†						
Knorringite[l]	Mg	Cr	1579.5	153	4.3	364	2.16	202	10.4	105	31.9
Grossular[a]	Ca	Al	1667.0	166	4.3	341	2.15	167	8.8	131	35.6
exp.				167[b]	5.46[b]	300[f]		220[f]		115[f]	
				168[m]	6.1[m]						
				175[h]	4.4[h]†						
				168[k]							
Uvarovite[l]	Ca	Cr	1737.1	143	4.7	337	2.00	170	9.9	105	34.4
exp.				162[k]	4.7[m]			257[c]			
Andradite[l]	Ca	Fe	1753.2	147	4.4	327	1.99	183	10.1	105	34.2
exp.				159.4[b]	5.85[b]						
				159[p]	4[p]†	200[p]		330[p]		160[p]	
				157[h]	5.1[h]†						
				158[n]							
Goldmanite[l]	Ca	V	1762.8	139	4.7	338	1.97	187	10.1	97	34.4
Khoharite[l]	Mg	Fe	1530.8	163	4.4	357	2.22	212	10.0	113	32.1
Blythite[l]	Mn	Mn	1683.7	150	4.8	390	2.04	173	10.3	109	32.1
exp.				152[q]	6.4[q]						
Skiagite[l]	Fe	Fe	1588.2	165	4.7	380	2.13	206	11.2	121	30.7
exp.				157[r]	6.7[r]						
Calderite[l]	Mn	Fe	1674.4	152	4.7	364	2.05	191	10.5	109	32.6
Katoite[s]	Ca	Al	1732.3	56	3.6	19	3.16	196	7.1	55	31.4
exp.				66[m]	4.1[m]						
				52[t]	4[t]†	50[t]				50[t]	

(*a*) Akhmatskaya *et al.* (1999), theoretical result; (*b*) Conrad *et al.* (1999), Brillouin spectroscopy, natural single crystals; (*c*) Langer *et al.* (1997), spectroscopic measurements; (*d*) Zhang *et al.* (1998), diamond anvil cell, single-crystal X-ray diffraction; (*e*) Sato *et al.* (1978), diamond anvil cell, powder X-ray diffraction, synthetic garnets; (*f*) Hazen & Finger (1978), diamond anvil cell, single-crystal X-ray diffraction; (*g*) Chen *et al.* (1999), high-pressure ultrasonic interferometry, polycrystal; (*h*) Zhang *et al.* (1999), diamond anvil cell, single-crystal X-ray diffraction, synthetic garnets; (*i*) Smith & Langer (1983), spectroscopic measurements; (*j*) Babuska *et al.* (1978), ultrasonic measurements on natural almandine-rich solid solution; (*k*) Bass (1989), Brillouin spectroscopy, natural single crystals; (*l*) present results; (*m*) Olijnyk *et al.* (1991), diamond anvil cell, powder X-ray diffraction, synthetic garnets; (*n*) Bass (1986), Brillouin spectroscopy; (*p*) Hazen & Finger (1989), diamond anvil cell, single-crystal X-ray diffraction; (*q*) Arlt *et al.* (1998), diamond anvil cell, single-crystal X-ray diffraction, synthetic garnets; (*r*) Woodland *et al.* (1999), diamond anvil cell, synthetic garnets; (*s*) Nobes *et al.* (2000), theoretical result; (*t*) Lager & von Dreele (1996), diamond anvil cell, powder X-ray diffraction, synthetic garnets. † Assumed value; fixed when fitting equation-of-state.

Gibbs (1971). A subsequent study of thermodynamic properties of skiagite reported the cell parameter as 11.72 (5) Å (Ostrovsky *et al.*, 1984). These authors also found a number of reflections that were forbidden in the $Ia\bar{3}d$ space group, so that a lower symmetry, $I2_13$, has been suggested for this garnet. None of the subsequent structural studies confirmed this symmetry reduction, however. Woodland & Ross (1994) carried out a detailed study of two solid-solution series, almandine–skiagite and andradite–skiagite. Their results confirmed that all Fe^{3+} ions are in octahedral coordination and Fe^{2+} ions are in dodecahedral coordination. The unit-cell parameter of the end-member skiagite garnet was determined as 11.7278 (6) Å (Woodland & O'Neill, 1993; Woodland & Ross, 1994). The stability range of skiagite was found to be from 9 to 13 GPa, in good agreement with the earlier estimates by Karpinskaya *et al.* (1982). The only experimental determination of the fractional coordinates of the O atom has been carried out for the 10% almandine–90% skiagite solid solution (Woodland & Ross, 1994) and the results are in good agreement with the theoretical data for the end-member skiagite, Table 8.

The bulk modulus and its pressure derivative for skiagite have been reported by Woodland *et al.* (1999) as 157.4 (3.0) GPa and 6.7 (8). We calculated these values as B = 165.0 (1.5) GPa and B' = 4.7 (2) from the fit of the calculated equation-of-state. The discrepancy between the theoretical and the experimental value for B' is as large as that observed in the calculations for blythite. There, however, the experimental and theoretically obtained bulk moduli were nearly identical, while for skiagite this is not the case. As has been discussed by Zhang *et al.* (1999), there exists a correlation between B and B', and hence here the different values may be caused by fitting the equation-of-state over different pressure ranges.

Table 8
Structure of skiagite at ambient pressure: cell parameters, fractional coordinates of the O atom and bond lengths.

	Theory	Experiment[(a)]
a (Å)	11.667	11.708 (2)
O_x	0.0365	0.0352 (1)
O_y	0.0570	0.0529 (1)
O_z	0.6604	0.6568 (1)
Fe^{3+}—O (Å)	2.033	1.981 (2)
Si—O (Å)	1.616	1.637 (2)
Fe^{2+}—O(1) (Å)	2.258	2.257 (2)
Fe^{2+}—O(2) (Å)	2.331	2.373 (2)

(*a*) Woodland & Ross (1994), 10% almandine–90% skiagite solid solution.

Table 9
Structure of calderite at ambient pressure: cell parameters, fractional coordinates of the O atom and bond lengths.

	Theory	Calculated[(a)]
a (Å)	11.875	11.84
O_x	0.0383	0.0367
O_y	0.0511	0.0518
O_z	0.6579	0.6562
Fe^{3+}—O (Å)	2.022	2.00
Si—O (Å)	1.621	1.64
Mn^{2+}—O(1) (Å)	2.307	2.30
Mn^{2+}—O(2) (Å)	2.437	2.42

(*a*) Novak & Gibbs (1971), empirical extrapolation.

3.8. Calderite

Calderite, $Mn_3^{2+}Fe_2^{3+}[SiO_4]_3$, is an end-member garnet closely related to skiagite and blythite. Dasgupta *et al.* (1987) reported up to 50% calderite content in the carbonatic rock from the Sausar Group, India, which is one of the highest calderite contents found in the natural garnets. Amthauer *et al.* (1989) found up to 36% of calderite in calderite–andradite garnets from Otjosondu, Namibia, and showed that calderite is usually accompanied by a small amount of blythite. Lattard & Schreyer (1983) carried out a detailed study of the mechanism of synthesis of calderite and reported structural and thermodynamical data for nearly pure calderite (it was not possible to eliminate a residual 1–4% of blythite or skiagite). Their reported lattice constant of 11.822 (1) Å agrees well with the data of Nishizawa *et al.* (1977), 11.821 Å, also obtained for a synthetic garnet. The calculation based on the equation of Novak & Gibbs (1971) gives 11.84 Å, again in good agreement with the experimental data. We have obtained a value of 11.875 Å for a pure end-member, which is very close to the experimental results. The calculated internal parameters for calderite, Table 9, agree well with the empirical prediction by Novak & Gibbs (1971).

We are not aware of any experimental study of the compression of calderite. One can expect, however, that the bulk modulus should be close to that of blythite and skiagite. We obtained B = 151.5 (2.0) GPa and B' = 4.74 (2), values which are much closer to the blythite results.

One should note that magnetic effects are expected to be the strongest in calderite out of all the Mn- and Fe-containing garnets studied here. The nominal high-spin state for both Mn^{2+} and Fe^{3+} ions is d^5, which produces five unpaired electrons per transition-metal ion. DFT calculations predict an ordered ferromagnetic ground state which is substantially more stable than the paramagnetic solution (approximately 0.5 eV per formula unit). This is an effect which is an order of magnitude larger on energetics than in such garnets as almandine or spessartine. Even if the DFT description of the magnetic state of these systems is inaccurate, this is still an indication that the spin ordering in calderite is more pronounced than in similar garnets and it would be very worthwhile to study the magnetic properties of this compound.

The effect of pressure on bond lengths and on polyhedral distortion parameters of Mn^{2+}-containing garnets is compared in Figs. 11 and 12, respectively. It is apparent that the qualitative descriptions of blythite and calderite are similar and that they are very different from that for the aluminosilicate garnet spessartine. In particular, the pressure dependence of the octahedra is similar to the results for the Mg-containing garnets pyrope, knorringite and khoharite, as can be seen from Figs. 10 and 12. The octahedra become monotonically more distorted upon compression. According to our results, it is more usual for octahedra to become more regular upon compression to a certain critical pressure, with the distortion indices then increasing again on further compression.

4. Discussion

4.1. Reliability of the model

Comparisons of the theoretical data obtained here with the experimental data published elsewhere are summarized in Table 7. They show that the quantum-mechanical model reproduces lattice parameters to within 1% and bulk moduli

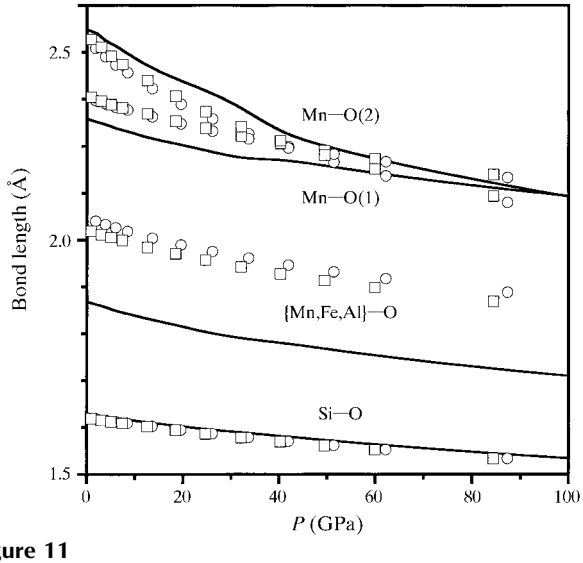

Figure 11
Calculated pressure dependence of bond lengths in blythite (circles), calderite (squares) and spessartine (solid lines, from Akhmatskaya *et al.*, 1999).

generally to within 10 GPa. This is remarkable for a static, fully ordered model. Such agreement implies that changes in structural parameters or elastic properties due to thermally induced X-site disorder, to different magnetic states, or to Jahn–Teller distortion of the coordination polyhedra can to first-order be neglected in the derivation of structure–property relations. The general applicability of the model is confirmed by the reproduction of rather subtle effects. Based on experimental values, Zhang *et al.* (1999) concluded that the pressure derivatives of the bulk moduli of andradite, pyrope, grossular, almandine and spessartine follow $B'(\text{an}) > B'(\text{py}) > B'(\text{gr}) > B'(\text{al}) \simeq B'(\text{sp})$, while our theoretical data give $4.4 > 4.3 \simeq 4.3 > 4.2 > 3.9$. This leads us to believe that in the one case where we observe a noticeable disagreement for elastic properties between experiment and theory, namely for uvarovite where the theoretical results for B differ by 20 GPa, it would be worthwhile to check the one available experimental value.

We are confident that the other predictions made in the present study with respect to structural parameters are also reliable. Specifically, we think that our results for pyrope and andradite, where experimental data are available (see Table 7), demonstrate that parameter-free model calculations can reliably be used to obtain the compressibility of coordination polyhedra. For example, Zhang *et al.* (1998) noted that the bulk modulus for CaO_8 dodecahedra in andradite was expected to be lower than that for MgO_8 dodecahedra in pyrope, which is indeed the case according to the theoretical data. The reliability of our model calculations then implies that those experimental values for the compressibility of coordination polyhedra that differ significantly from our results are probably inaccurate. Hence, the values derived from diffraction experiments for B_{YO_6} for andradite and grossular should be reassessed. This is very likely also the case for the low value of B = 200 GPa for the SiO_4 tetrahedra in andradite obtained by Hazen & Finger (1989). On the other hand, Zhang *et al.* (1998) obtained B = 580 GPa for the SiO_4 tetrahedra in pyrope, an unrealistically high value.

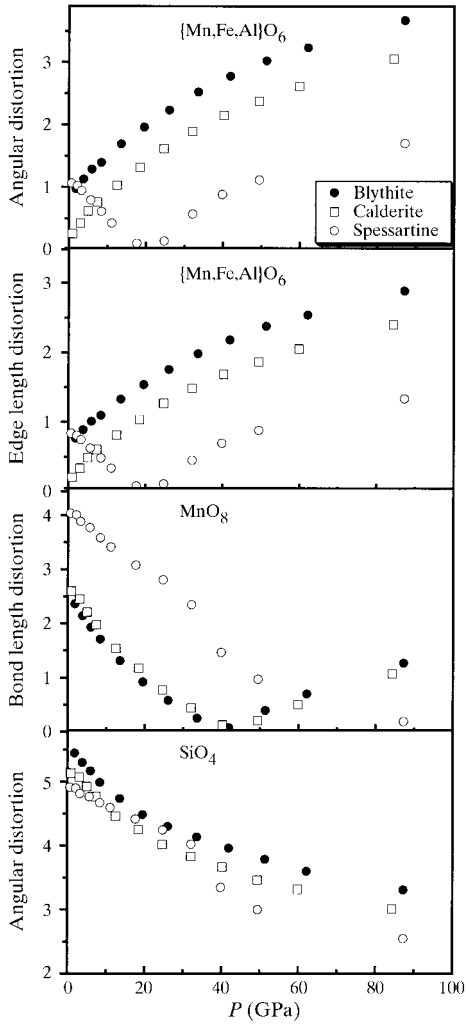

Figure 12
Pressure dependence of polyhedral distortions in blythite (solid circles), calderite (squares) and spessartine (open circles, from Akhmatskaya *et al.*, 1999).

The derivation of polyhedral compression moduli from optical spectroscopic measurements can only give semi-quantitative results. This is illustrated by the comparison between available spectroscopic results for polyhedral stiffnesses and the data obtained from X-ray diffraction or from the present theoretical study (Table 7). For uvarovite, two values which differ significantly have been presented in the literature (Langer *et al.*, 1997; Burns, 1987). Even the more recent value of B_{YO_6} = 257 (32) GPa from Langer *et al.* (1997), which is already much smaller than the older value, 453 GPa, from Burns (1987) is still 80 GPa larger than the value obtained here. Similarly, B_{YO_6} obtained from optical spectroscopic measurements for pyrope (Langer *et al.*, 1997) is more than 50 GPa larger than the experimentally and theoretically obtained values (Table 7). The discrepancy might be attributed to the use of Cr^{3+} as a probe. This choice of a probe may introduce a systematic error due to the local distortions around Cr^{3+}, which effectively constitutes a defect in the pyrope structure. In contrast to the significant overestimation of B_{YO_6} in uvarovite and grossular, the corresponding value for almandine (Smith & Langer, 1983) is 90 GPa smaller than the value obtained here.

For those compounds which have Jahn–Teller distorted octahedra, the current model underestimates the change of the compressibility as a function of pressure. However, more experimental data are required to establish for which compounds this is problematic.

4.2. Correlation between composition, structure, bulk modulus and polyhedral compressibility

The data compiled in Table 7 can be used to investigate systematic trends that might be present in this family of minerals. The end-member hydrogrossular, katoite, is included in this compilation to illustrate the effect of a hydrogarnet substitution on compressibility.

The availability of the bulk moduli of 12 silicate garnet end-members allows us to investigate correlations between properties which cannot easily be discovered when only the few

Table 10
Interatomic distances, ionic radii according to Shannon (1976), the difference between calculated distances and the sum of ionic radii, and theoretical bulk moduli for garnets studied here and elsewhere (Akhmatskaya *et al.*, 1999; Nobes *et al.*, 2000).

See text for an explanation of the notation.

Garnet	X	Y	$X-O$ (Å)	$Y-O$ (Å)	R_X (Å)	R_Y (Å)	R_X/R_Y	$\Delta(X-O)$ (Å)	$\Delta(Y-O)$ (Å)	B (GPa)	B_{YO_6} (GPa)	B_{XO_8} (GPa)
Pyrope	Mg	Al	2.28	1.85	0.89	0.54	1.65	+0.01	−0.07	170	204	127
Almandine	Fe	Al	2.32	1.86	0.92	0.54	1.70	+0.02	−0.07	177	213	121
Spessartine	Mn	Al	2.35	1.87	0.96	0.54	1.78	+0.01	−0.05	183	182	141
Grossular	Ca	Al	2.43	1.90	1.12	0.54	2.07	−0.07	−0.02	166	167	131
Knorringite	Mg	Cr	2.31	1.98	0.89	0.62	1.44	+0.04	−0.02	153	202	105
Uvarovite	Ca	Cr	2.44	2.01	1.12	0.62	1.81	−0.06	+0.01	143	170	105
Andradite	Ca	Fe	2.44	2.02	1.12	0.65	1.72	−0.06	−0.01	147	183	105
Goldmanite	Ca	V	2.45	2.03	1.12	0.64	1.75	−0.05	+0.01	139	187	97
Khoharite	Mg	Fe	2.29	1.93	0.89	0.65	1.37	+0.02	−0.10	163	212	113
Blythite	Mn	Mn	2.37	2.05	0.96	0.64	1.50	+0.02	+0.03	150	173	109
Calderite	Mn	Fe	2.37	2.02	0.96	0.65	1.48	+0.03	−0.01	152	191	109
Skiagite	Fe	Fe	2.29	2.03	0.92	0.65	1.42	−0.01	0.00	165	206	121
Katoite	Ca	Al	2.34	1.88	1.12	0.54	2.07	−0.16	−0.04	56	196	55

available experimental data are used. For example, our data show that the volume dependence of B can be reasonably well described by a linear relationship (Fig. 13), while a fit based on a simple proportionality between B and $1/V$ results in a very poor description of the computed data.

It is instructive to analyze the correlation between bulk moduli of the individual polyhedra and that of the whole crystal. It follows from Table 7 that there is no statistical correlation between the overall bulk modulus of the structure and the bulk moduli of the tetrahedra or octahedra. On the other hand, there is a well defined linear correlation between the modulus of the dodecahedra and that of the crystal, see Fig. 14(*a*). Furthermore, if we add the bulk moduli of the individual polyhedra weighted by their relative volumes, the calculated 'average' polyhedral bulk modulus has an even better linear correlation with the calculated bulk modulus of the garnet structure, Fig. 14(*b*). As the dodecahedra are more rigid in aluminosilicate garnets than in any other garnets studied here, the strong correlation between the bulk modulus of dodecahedra and that of the complete structure explains why pyralspites are less compressible than ugrandites (see Table 7).

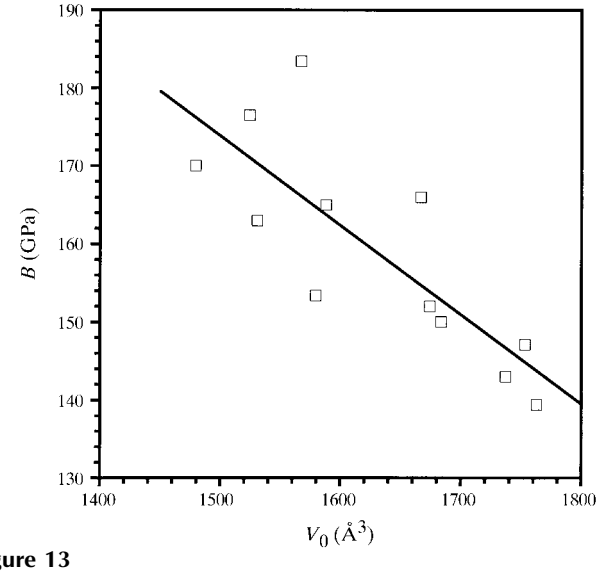

Figure 13
Correlation between the cell volume and the bulk modulus of 12 garnets (calculated data).

Finally, let us analyze the results for bulk moduli in terms of ionic radii of cations. Table 10 presents theoretical results for 13 garnets. We show the average $X-O$ distance, the $Y-O$ distance, ionic radii for both X and Y cations (Shannon, 1976) and their ratio. We also present the differences between calculated cation–oxygen distances and the sum of corresponding atomic radii, *i.e.* $\Delta(X-O) = |X-O| - R_X - R_O$. We did not include the data for tetrahedra since Si—O distances are essentially the same in all garnets. The sum of the ionic radii predicts this distance to be 1.64 Å and the calculated values for all the garnets can be represented as 1.63 (1) Å.

There are very few reliable correlations between the ionic radii presented in Table 10 and calculated bulk moduli. For example, the bulk modulus of octahedra in garnets with the same trivalent cation Y seems to be determined by the value of $\Delta(Y-O)$: the smaller this value, the higher the bulk modulus. This explains in particular why knorringite is less compressible than uvarovite. On the other hand, the value of $\Delta(X-O)$ in garnets with the same divalent cation X has little effect on the bulk modulus of dodecahedra. In addition, the values of $\Delta(X-O)$ are more uniform: 0.01–0.04 for Mg, −0.05 to −0.07 for Ca, 0.01–0.03 for Mn, −0.01 to 0.02 for Fe. This shows that the nature of the divalent cation has a stronger effect on the local geometry around the trivalent cation than the other way round.

4.3. Compression mechanism

There are two major compression mechanisms to be considered for garnets, namely, bond compression and bond bending. SiO_4 tetrahedra are very stiff, so the only bond compression that can take place would be related to the YO_6 octahedra and XO_8 dodecahedra. We have mentioned already that a more efficient compression mechanism in silicate garnets is polyhedral rotation. This rotation can be expressed

quantitatively as the change in the Si—O—Y angle. The polyhedra distortion indices that measure the deviation of polyhedra from their ideal shape were found to depend linearly on the change of the Si—O—Y angle in aluminosilicate garnets (Zhang *et al.*, 1998; Akhmatskaya *et al.*, 1999).

The results presented in this paper show that the previously reported trend (Zhang *et al.*, 1998; Akhmatskaya *et al.*, 1999) for the SiO_4 tetrahedron and for the XO_8 dodecahedron to become more regular on compression is a general one. It appears that it is the response of the YO_6 octahedra to pressure that defines individual features of compressibility of various garnets. The octahedra in spessartine, andradite, uvarovite and goldmanite attain a regular shape at a moderate pressure and they become distorted on further compression. The octahedra in pyrope, almandine, blythite, skiagite, calderite, knorringite and khoharite become more distorted under pressure. Grossular is the only garnet where the octahedra become less distorted over the whole pressure range studied.

Fig. 15 shows that there is an accurate linear correlation in all garnets between the normalized distortion parameters for XO_8 polyhedra and the relative change of the Si—O—Y angle. We also present in Fig. 15 the results of the linear fit for aluminosilicate garnets as derived by Akhmatskaya *et al.* (1999). The results for the Ca-containing garnets uvarovite, andradite and goldmanite are found to follow this line quite closely. Knorringite, khoharite, calderite, blythite and especially skiagite exhibit different slopes of the linear dependence. We suggest that this difference is related to the value of the ratio of the ionic radii of X and Y cations, see Table 10. All garnets which are characterized by the same slope in Fig. 15 have a ratio of R_X/R_Y greater than 1.65. This ratio is less than 1.50 for all the garnets with a different slope of the plot in Fig. 15. This shows that the trivalent Cr, Fe and Mn cations are quite large for the octahedral cavity they occupy so that knorringite, khoharite, calderite, blythite and skiagite are close to the stability limit of cubic garnets (Novak & Gibbs, 1971). Even at ambient pressure the octahedra in the above-mentioned garnets are more distorted than in other garnets. Apparently, only the presence of Ca as a divalent cation expands the lattice sufficiently to accommodate these transition-metal cations in octahedra.

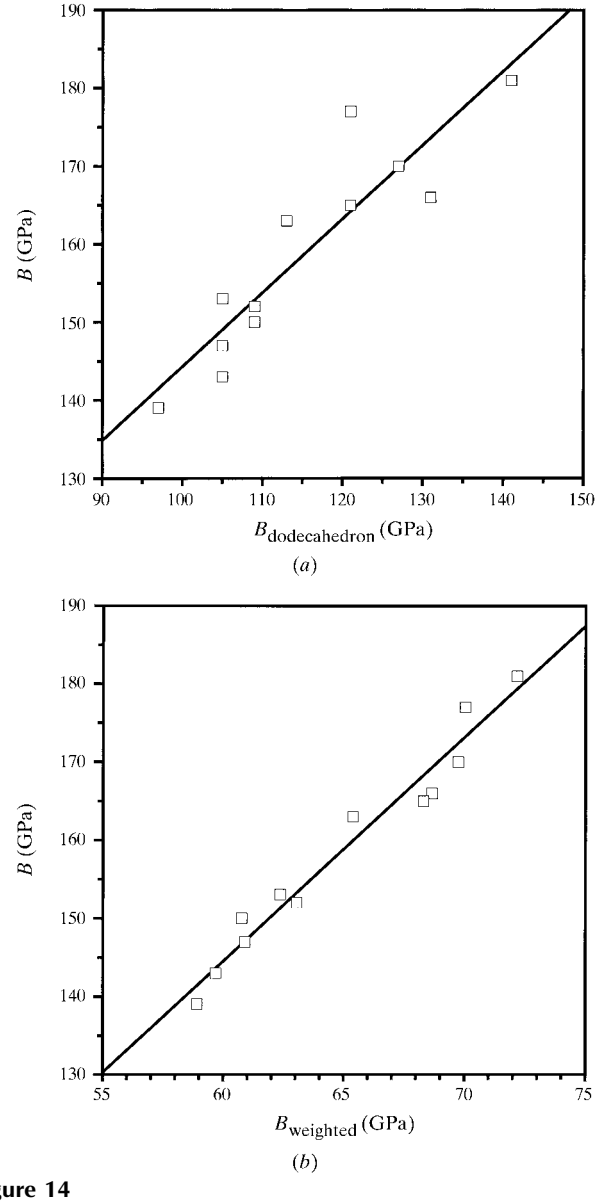

Figure 14
Correlation between the calculated bulk modulus and (*a*) bulk modulus of dodecahedron and (*b*) weighted sum of polyhedral bulk moduli.

5. Conclusions

This study has served a dual purpose: to provide reliable data for structures and properties of an important family of

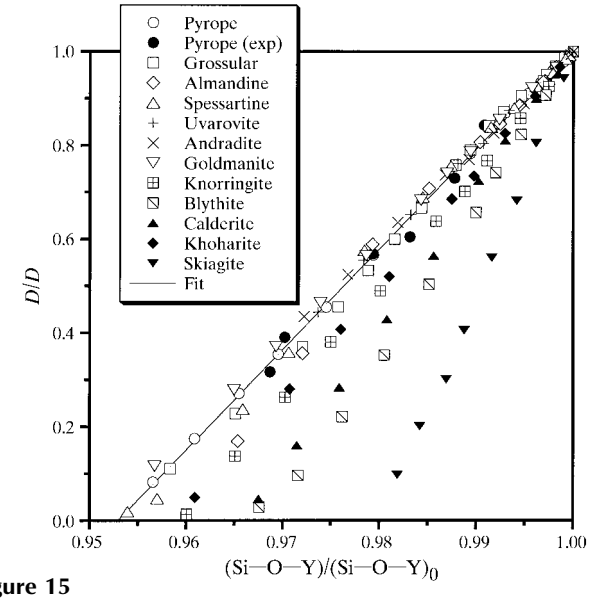

Figure 15
Correlation between the normalized bond length distortion parameters for XO_8 polyhedra and the relative change of the Si—O—Y angle. Experimental data for pyrope are from Zhang *et al.* (1998), theoretical data for pyrope, grossular, almandine and spessartine are from Akhmatskaya *et al.* (1999). Solid line – linear fit for aluminosilicate garnets (Akhmatskaya *et al.*, 1999).

minerals and to illustrate the current capabilities of density functional based modeling of complex inorganic solids.

We presented a detailed *ab initio* study of ground-state properties and of pressure-induced structural changes of eight garnets. These results together with the earlier findings for aluminosilicate garnets are used to analyze the compression mechanism in terms of bond compression and bond bending. A consistent picture emerges of the framework compression being dominated by the bending of the tetrahedron–octahedron angle.

The role of ionic radii of both divalent and trivalent cations has been analyzed in terms of their effect on crystal stability and on the bulk modulus. We showed that the bulk modulus of a garnet is strongly affected by the bulk modulus of the dodecahedra, while compressibility of other individual polyhedra displays no correlation with the compressibility of the structure as a whole.

One of the virtues of the parameter-free modeling approach used here is that the behavior of the structure at high compressions can be reliably predicted. This is generally not the case for models based on empirical potentials. Specifically, we predict in several cases a non-trivial behavior of the change of the polyhedral distortion as a function of pressure. The experimental verification of these results is challenging, but should be possible with high-pressure experiments using diamond-anvil cells at third generation synchrotron sources.

A number of further issues are now open to *ab initio* treatment. Suggested applications might include the energetics of garnets, characterization of defects, lattice dynamical study of vibrational properties, the role of magnetic effects in garnets containing 3*d* metals as cations, the underlying reasons for the absence of a symmetry-breaking ordered Jahn–Teller distortion in Mn^{3+}-bearing garnets, *etc*. The major problem with the application of *ab initio* results to explain the properties of garnets is that these minerals tend to exist as solid solutions. Recent theoretical developments seem to make possible the study of mixing properties in the virtual crystal approximation (Bellaiche & Vanderbilt, 2000). In summary, the present study establishes the density functional approach as a reliable modeling technique for garnets and related materials.

References

Akhmatskaya, E. V., Nobes, R. H., Milman, V. & Winkler, B. (1999). *Z. Kristallogr.* **214**, 808–819.

Amthauer, G., Katz-Lehnert, K., Lattard, D., Okrusch, M. & Woermann, E. (1989). *Z. Kristallogr.* **189**, 43–56.

Arlt, T., Armbruster, T., Miletich, R., Ulmer, P. & Peters, T. (1998). *Phys. Chem. Miner.* **26**, 100–106.

Armbruster, T. & Geiger, C. A. (1993). *Eur. J. Mineral.* **5**, 59–71.

Arni, R., Langer, K. & Tillmanns, E. (1985). *Phys. Chem. Miner.* **12**, 279–282.

Babuska, V., Fiala, J., Kumazawa, M., Ohno, I. & Sumino, Y. (1978). *Phys. Earth Planet. Inter.* **16**, 157–176.

Bass, J. D. (1986). *J. Geophys. Res.* **91**, 7505–7516.

Bass, J. D. (1989). *J. Geophys. Res.* **94**, 7621–7628.

Baur, W. H. (1974). *Acta Cryst.* B**30**, 1195–1215.

Bellaiche, L. & Vanderbilt, D. (2000). *Phys. Rev. B*, **61**, 7877–7882.

Benkerrou, C. & Fonteilles, M. (1989). *Am. Mineral.* **74**, 852–858.

Birch, F. (1978). *J. Geophys. Res.* **83**, 1257–1268.

Burns, R. G. (1987). *High-Pressure Research in Mineral Physics*, edited by M. H. Manghnani and Y. Syono, pp. 361–369, Geophysical Monograph 39, Mineral Physics 2. Washington: American Geophysical Union.

Carda, J., Monros, G., Esteve, V. & Amigo, J. M. (1994). *J. Solid State Chem.* **108**, 24–28.

Chen, G. L., Cooke, J. A., Gwanmesia, G. D. & Liebermann, R. C. (1999). *Am. Mineral.* **84**, 384–388.

Coes, L. Jr (1955). *J. Am. Ceram. Soc.* **38**, 298.

Conrad, P. G., Zha, C.-S., Mao, H.-K. & Hemley, R. J. (1999). *Am. Mineral.* **84**, 374–383.

Dasgupta, S., Bhattacharya, P. K., Banerjee, H., Fukuoka, M., Majumdar, N. & Roy, S. (1987). *Mineral. Mag.* **51**, 577–583.

Fermor, L. L. (1938). *Rec. Geol. Survey India*, **73**, 145–156.

Fursenko, B. A. (1980). *Dokl. Akad. Nauk SSSR*, **250**, 940–945.

Fursenko, B. A. (1983). *Dokl. Akad. Nauk SSSR*, **268**, 421–424.

Geller, S. (1967). *Z. Kristallogr.* **125**, 1–47.

Gentile, A. L. & Roy, R. (1960). *Am. Mineral.* **45**, 701–711.

Hallsworth, C. R., Livingstone, A. & Morton, A. C. (1992). *Mineral. Mag.* **56**, 117–120.

Hazen, R. M. & Finger, L. W. (1978). *Am. Mineral.* **63**, 297–303.

Hazen, R. M. & Finger, L. W. (1989). *Am. Mineral.* **74**, 352–359.

Hohenberg, P. & Kohn, W. (1964). *Phys. Rev.* **136**, 864–871.

Irifune, T., Ohtani, E. & Kumazawa, M. (1982). *Phys. Earth Planet. Inter.* **27**, 263–272.

Jeong, G. Y. & Kim, Y. H. (1999). *Mineral. Mag.* **63**, 253–256.

Karpinskaya, T. B., Ostrovsky, I. A. & Evstigneeva, T. L. (1982). *Izv. Vuzov AN SSSR. Geol.* **9**, 128–129.

Kingma, K. J. & Downs, J. W. (1989). *Am. Mineral.* **74**, 1307–1316.

Kohn, W. & Sham, L. J. (1965). *Phys. Rev. A*, **140**, 1133–1138.

Lager, G. A. & Von Dreele, R. B. (1996). *Am. Mineral.* **81**, 1097–1104.

Langer, K., Taran, M. N. & Platonov, A. V. (1997). *Phys. Chem. Miner.* **24**, 109–114.

Lattard, D. & Schreyer, W. (1983). *Contrib. Mineral. Petrol.* **84**, 199–214.

Leger, J. M., Redon, A. M. & Chateau, C. (1990). *Phys. Chem. Miner.* **17**, 161–167.

Leitner, B. J., Weidner, D. & Liebermann, R. C. (1980). *Phys. Earth Planet. Inter.* **22**, 111–121.

Lin, J. S., Qteish, A., Payne, M. C. & Heine, V. (1993). *Phys. Rev. B*, **47**, 4174–4180.

Louie, S. G., Froyen, S. & Cohen, M. L. (1982). *Phys. Rev. B*, **26**, 1738–1742.

Mill', B. V. (1964). *Dokl. Akad. Nauk SSSR*, **156**, 814–816.

Milman, V., Winkler, B., White, J. A., Pickard, C. J., Payne, M. C., Akhmatskaya, E. V. & Nobes, R. H. (2000). *Int. J. Quant. Chem.* **77**, 895–910.

Molecular Simulations Inc. (1998). *CASTEP User's Guide.* Molecular Simulations Inc., San Diego, CA.

Murad, E. (1984). *Am. Mineral.* **69**, 722–724.

Nishizawa, H., Shimada, M., Matsuoka, K. & Koizumi, M. (1977). *Bull. Chem. Soc. Jpn*, **50**, 3186–3188.

Nobes, R. H., Akhmatskaya, E. V., Milman, V., White, J. A., Winkler, B. & Pickard, C. J. (2000). *Am. Mineral.* **85**, 1706–1715.

Novak, G. A. & Gibbs, G. V. (1971). *Am. Mineral.* **56**, 791–825.

Ohashi, H., Fujita, T. & Osawa, T. (1981). *J. Jpn. Assoc. Mineral. Petrol. Econ. Geol.* **76**, 58–60.

Ohashi, H., Osawa, T. & Sato, A. (1995). *Acta Cryst.* C**51**, 2213–2215.

Olijnyk, H., Paris, E., Geiger, C. A. & Lager, G. A. (1991). *J. Geophys. Res.* **96**, 14313–14318.

Ostrovsky, I. A., Karpinskaya, T. B., Evstigneeva, T. L. & Mokhov, A. V. (1984). *Izv. Vuzov AN SSSR Geol.* **6**, 100–105.

Payne, M. C., Teter, M. P., Allan, D. C., Arias, T. A. & Joannopoulos, J. D. (1992). *Rev. Mod. Phys.* **64**, 1045–1097.

Perdew, J. P. & Wang, Y. (1992). *Phys. Rev. B*, **45**, 13244–13249.

Pilati, T., Demartin, F. & Gramaccioli, C. M. (1996). *Acta Cryst.* B**52**, 239–250.
Quareni, S. & de Pieri, R. (1966). *Mem. Accad. Patavina Sci. Lett. Arti Padua*, **78**, 151–170.
Renner, B. & Lehmann, G. (1986). *Z. Kristallogr.* **175**, 43–59.
Ringwood, A. E. (1977). *Earth Planet. Sci. Lett.* **36**, 443–448.
Sato, Y., Akaogi, M. & Akimoto, S. I. (1978). *J. Geophys. Res.* **83**, 335–338.
Shannon, R. D. (1976). *Acta Cryst.* A**32**, 751–767.
Sinogeikin, S. V. & Bass, J. D. (1999). *Phys. Rev. B*, **59**, 14141–14144.
Smith, G. & Langer, K. (1983). *Neues Jahrb. Mineral. Monatsh.* **12**, 541–555.
Strens, R. G. J. (1965). *Am. Mineral.* **50**, 260.
Vanderbilt, D. (1990). *Phys. Rev. B*, **41**, 7892–7895.
Wang, Z., Yagi, T. & Kondo, T. (1999). *J. Phys. Chem. Solids*, **60**, 441–444.
White, J. A. & Bird, D. M. (1994). *Phys. Rev. B*, **50**, 4954–4957.
Winkler, B. (1999). *Z. Kristallogr.* **214**, 506–527.
Woodland, A. B., Angel, R. J., Koch, M., Kunz, M. & Miletich, R. (1999). *J. Geophys. Res.* **104**, 20049–20058.
Woodland, A. B. & O'Neill, H. S. C. (1993). *Am. Mineral.* **78**, 1002–1015.
Woodland, A. B. & Ross II, C. R. (1994). *Phys. Chem. Miner.* **21**, 117–132.
Zhang, L., Ahsbahs, H. & Kutoglu, A. (1998). *Phys. Chem. Miner.* **25**, 301–307.
Zhang, L., Ahsbahs, H., Kutoglu, A. & Geiger, C. A. (1999). *Phys. Chem. Miner.* **27**, 52–58.